RSC Advances

PAPER

View Article Online
View Journal | View Issue

Cite this: *RSC Adv.*, 2026, **16**, 21510

Design, synthesis and bioactivity of indobufen derivatives

Danli Yuan,†[b] Liping Chen,†[c] Xin Huang,†[b] Jinquan Zhang *[b] and Ziyan Meng*[a]

Osteoporosis is characterized by excessive osteoclast-mediated bone resorption, a process that can be amplified by inflammatory cues within the bone microenvironment. Targeting the inflammation–osteoclast axis has therefore emerged as a promising strategy for preventing pathological bone loss. Here, a series of indobufen-modified derivatives were rationally designed and synthesized, and their biological activities were evaluated through a stepwise *in vitro* screening workflow. Early inflammatory profiling in fibroblast-like synoviocytes (FLS) identified compound **A1** as a lead candidate with pronounced suppression of pro-inflammatory mediators and matrix-degrading enzymes. In a RANKL-induced RAW264.7 osteoclastogenesis model, **A1** inhibited osteoclast maturation at non-cytotoxic concentrations, markedly reducing the expression of osteoclast functional proteins (MMP9 and cathepsin K) and disrupting F-actin ring formation and multinucleation. Collectively, these findings demonstrate that indobufen scaffold modification can yield small molecules with dual anti-inflammatory and anti-osteoclastogenic activities and highlight **A1** as a promising lead compound for the development of therapeutics targeting osteoporosis and inflammation-associated bone loss.

Received 8th March 2026
Accepted 13th April 2026

DOI: 10.1039/d6ra01985d

rsc.li/rsc-advances

1 Introduction

As a systemic skeletal disease, osteoporosis is defined by decreased bone mass and disrupted bone microstructure, directly heightening bone fragility and fracture risk.[1,2] Globally, its prevalence stands at around 18.3%, and incidence increases exponentially with age.[3–5] Bone integrity relies on the dynamic balance of bone remodeling, a process driven by osteoblast-mediated bone formation and osteoclast-mediated bone resorption.[6] Disruption of this balance—with bone resorption predominating—triggers osteoporosis. Multiple studies confirm that excessive activation and abnormal proliferation of osteoclasts are the primary drivers of pathological bone loss.[7] Osteoclasts derive from hematopoietic monocyte/macrophage precursors, and their maturation is tightly regulated by microenvironmental signaling molecules.[8] The binding of receptor activator of nuclear factor κB ligand (RANKL) to its receptor RANK on the surface of osteoclast precursors represents a key step in initiating osteoclast differentiation, fusion, and functional activation.[9] This interaction activates downstream transcription factors (NF-κB, NFATc1), thereby upregulating the expression of critical bone resorption-related enzymes such as tartrate-resistant acid phosphatase (TRAP) and cathepsin K. Targeting and inhibiting RANKL signaling pathway-mediated osteoclastogenesis is therefore a core strategy for the prevention and treatment of osteoporosis.[10–13]

Clinically used anti-osteoporotic drugs are primarily categorized into two classes: anti-resorptive agents and bone-forming agents. Anti-resorptive drugs, including bisphosphonates and denosumab, inhibit osteoclast-mediated bone resorption and have been proven effective in reducing fracture risk, but long-term administration carries safety concerns.[14] For instance, long-term bisphosphonate use may lead to rare adverse effects such as atypical femoral fractures and osteonecrosis of the jaw, while certain regimens also increase infection risk.[15] Bone-forming agents, such as parathyroid hormone analogs, exert their effects by stimulating osteoblast-mediated new bone formation. Despite demonstrated efficacy, their high cost, limited treatment duration, and potential side effects[16] underscore the urgent need for a novel therapeutic approach with high efficacy, excellent safety, and affordability. Because of these drawbacks, there is a clear need for novel therapies that can safely reduce osteoclast-driven bone resorption without incurring serious adverse effects.

Drug repurposing and structural modification of existing drugs offer a fast-track route in the search for new osteoporosis treatments. Using known drugs as starting points is efficient since their pharmacological and safety profiles are already well documented.[17] In this study, we explored the repurposing of indobufen, a drug originally developed as an antiplatelet cyclooxygenase inhibitor for cardiovascular conditions.

[a]*Key Laboratory of Green and Healthy Livestock and Poultry Breeding Technology of Jiangxi Education Institutes, Ganzhou Polytechnic College, Ganzhou, 341000, China. E-mail: mengzy@gzpt.edu.cn*
[b]*Gannan Medical University, Ganzhou, 341000, China*
[c]*Ganzhou People's Hospital, Ganzhou, 341000, China*
† These authors contributed equally to this work.

Indobufen, as a reversible cyclooxygenase inhibitor, exerts significant anticoagulant and anti-inflammatory activities by blocking the biosynthesis of thromboxane and prostaglandins.[18] Scheme 1 details the arachidonic acid (AA) biochemical pathway and the selective, reversible inhibitory action of indobufen, a non-steroidal antiplatelet agent. Arachidonic acid is first released from cell membrane phospholipids *via* the enzyme phospholipase A_2 (PLA_2). Free AA then enters three major metabolic branches: the cyclooxygenase (COX) pathway (cyan), the lipoxygenase (LOX) pathway (green), and the cytochrome P450 (CYP) pathway (blue). Indobufen acts exclusively on the COX pathway: it functions as a reversible, non-competitive inhibitor of cyclooxygenase-1 (COX-1), blocking the conversion of AA to prostaglandin G_2/H_2 (PGG_2/PGH_2) in platelets, while sparing COX-2 activity.[19] Epidemiological and pathological evidence indicates a close "immune–bone" interaction between chronic inflammation and osteoporosis. Particularly in pathological conditions such as rheumatoid arthritis, elevated levels of prostaglandin E2 and inflammatory cytokines (*e.g.*, IL-1β, IL-6) in the synovial microenvironment upregulate the expression of Receptor Activator of Nuclear Factor-κB Ligand (RANKL) on fibroblast-like synoviocytes. This disruption of bone remodeling directly drives abnormal osteoclast differentiation and bone erosion.[20] Based on the potential of indobufen to inhibit the COX/PGE2 axis, we propose a medicinal chemistry optimization strategy: to develop a class of dual-acting bone protective agents that simultaneously target the inflammatory microenvironment and osteoclastogenesis through structural modification of the indobufen scaffold.

To validate this structure–activity relationship hypothesis, this study designed and synthesized 10 novel indobufen derivatives and established a dual *in vitro* screening model encompassing the "inflammatory microenvironment" and the "bone resorption endpoint." In a co-culture system of FLS cells and RANKL-induced RAW264.7 macrophages, we precisely evaluated the transcriptional inhibitory activity of candidate molecules on osteoclast-specific genes (Ctsk, Acp5, Mmp9) using quantitative PCR (qPCR). The screening results identified compound **A1** as the most promising lead compound. Cell cytotoxicity experiments confirmed that **A1** exhibited excellent safety within its effective pharmacological concentration range without significant cytotoxicity and dose-dependently inhibited osteoclast phenotypic formation. We further elucidated the molecular targets of **A1** through follow-up mechanistic studies. Western blot analysis revealed that **A1** potently blocks RANKL-induced phosphorylation cascades in the MAPK pathway—encompassing the p-ERK, p-JNK, and p-p38 subgroups—and simultaneously inhibits the NF-κB signaling pathway.[21] Laser confocal microscopy experiments confirmed that **A1** effectively suppresses the cytoplasmic-to-nuclear translocation of NFATc1 (nuclear factor of activated T-cells, cytoplasmic 1), a key transcription factor orchestrating osteoclast differentiation.[22,23] Collectively, this study characterizes **A1**, a novel indobufen derivative, as exerting robust anti-osteoclastogenic activity *in vitro* by targeting the NF-κB/MAPK/NFATc1 signaling axis. These findings support targeted modification of the indobufen scaffold as a viable strategy for developing therapies against inflammatory bone loss diseases. Notably, **A1**, a highly promising candidate, warrants rigorous *in vivo* pharmacodynamic and pharmacokinetic evaluations.

2 Results and discussion

2.1 Synthesis of Indobufen derivatives A1–A10

In the present study, a series of Indobufen derivatives was rationally designed and synthesized. Compounds **A1–A4** were obtained *via* a cyclization reaction between stoichiometric

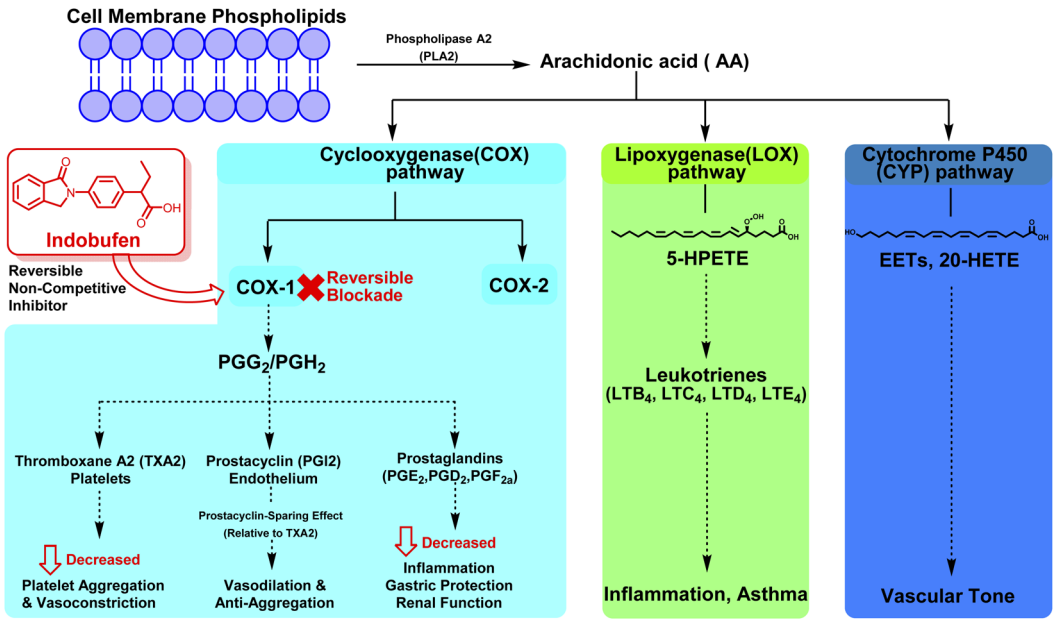

Scheme 1 Indobufen interacts the arachidonic acid biochemical pathway.

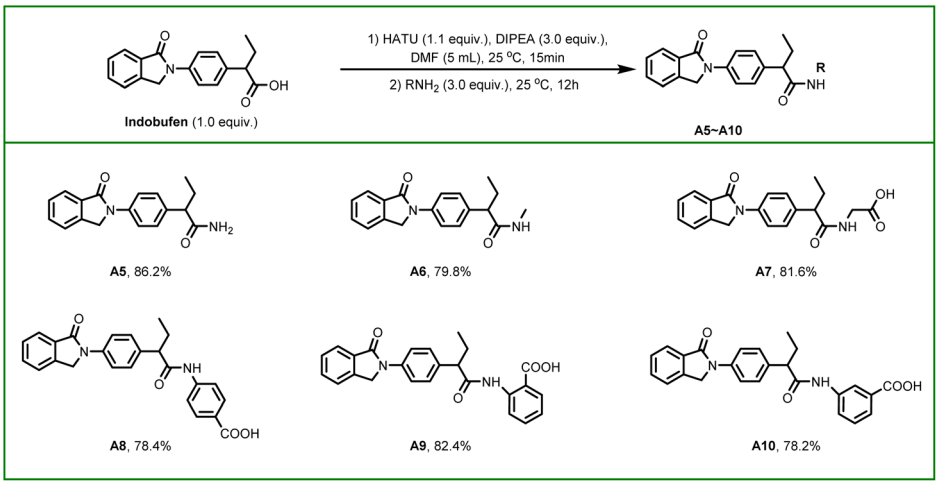

Scheme 2 Synthesis of indobufen derivatives (A1–A4).

amounts of *o*-carboxybenzaldehyde (1 equiv.) and substituted anilines (1.1 equiv.), followed by ester hydrolysis, as illustrated in Scheme 2. Additionally, indobufen derivatives **A5–A10** were prepared through a condensation reaction between Indobufen and corresponding amine derivatives, as depicted in Scheme 3. The yield of synthesized derivatives ranged from 78% to 87%.

2.2 Screening of indobufen derivatives

To preliminarily evaluate the anti-inflammatory potential of the synthesized indobufen-derived compounds, fibroblast-like synoviocytes (FLS) were treated with derivatives **A1–A10** (20 μM) during inflammatory stimulation for 6 h, followed by RT-qPCR analysis of cytokines and matrix/remodeling-associated genes. As shown in Fig. 1, inflammatory stimulation markedly increased the mRNA expression of interleukin-1β (IL-1β, Fig. 1A and B) and interleukin-6 (IL-6, Fig. 1C and D), as well as intercellular adhesion molecule 1 (ICAM1, Fig. 1E and F) and matrix metalloproteinase 9 (MMP9, Fig. 1G and H), compared with the NC group, confirming successful induction of an inflammatory response in FLS cells. Among the tested compounds, several derivatives exhibited varying degrees of inhibitory effects on inflammatory gene expression. Notably, treatment with **A1** resulted in a consistent and significant reduction in the mRNA levels of IL-1β and IL-6 compared with the stimulated group, whereas most other derivatives showed limited or inconsistent effects. In addition, **A1** markedly suppressed the expression of MMP9, a key mediator associated with extracellular matrix degradation, while exerting minimal influence on ICAM1 expression, suggesting a selective anti-inflammatory profile. In contrast, other indobufen-modified derivatives displayed either marginal inhibitory activity or no statistically significant effects on the examined inflammatory markers. Based on its superior and consistent inhibitory effects on pro-inflammatory cytokines and matrix-degrading enzymes, **A1** was identified as a lead candidate for further evaluation. Collectively, these results demonstrate that **A1** exhibits a favorable anti-inflammatory profile in FLS cells during early inflammatory stimulation. Therefore, **A1** was selected for subsequent mechanistic investigations in RAW264.7 cells to further explore its therapeutic

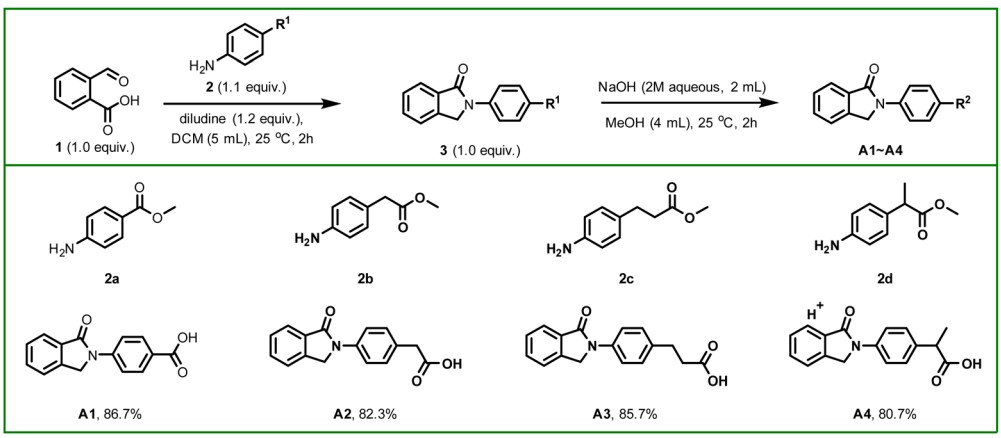

Scheme 3 Synthesis of indobufen derivatives (A5–A10).

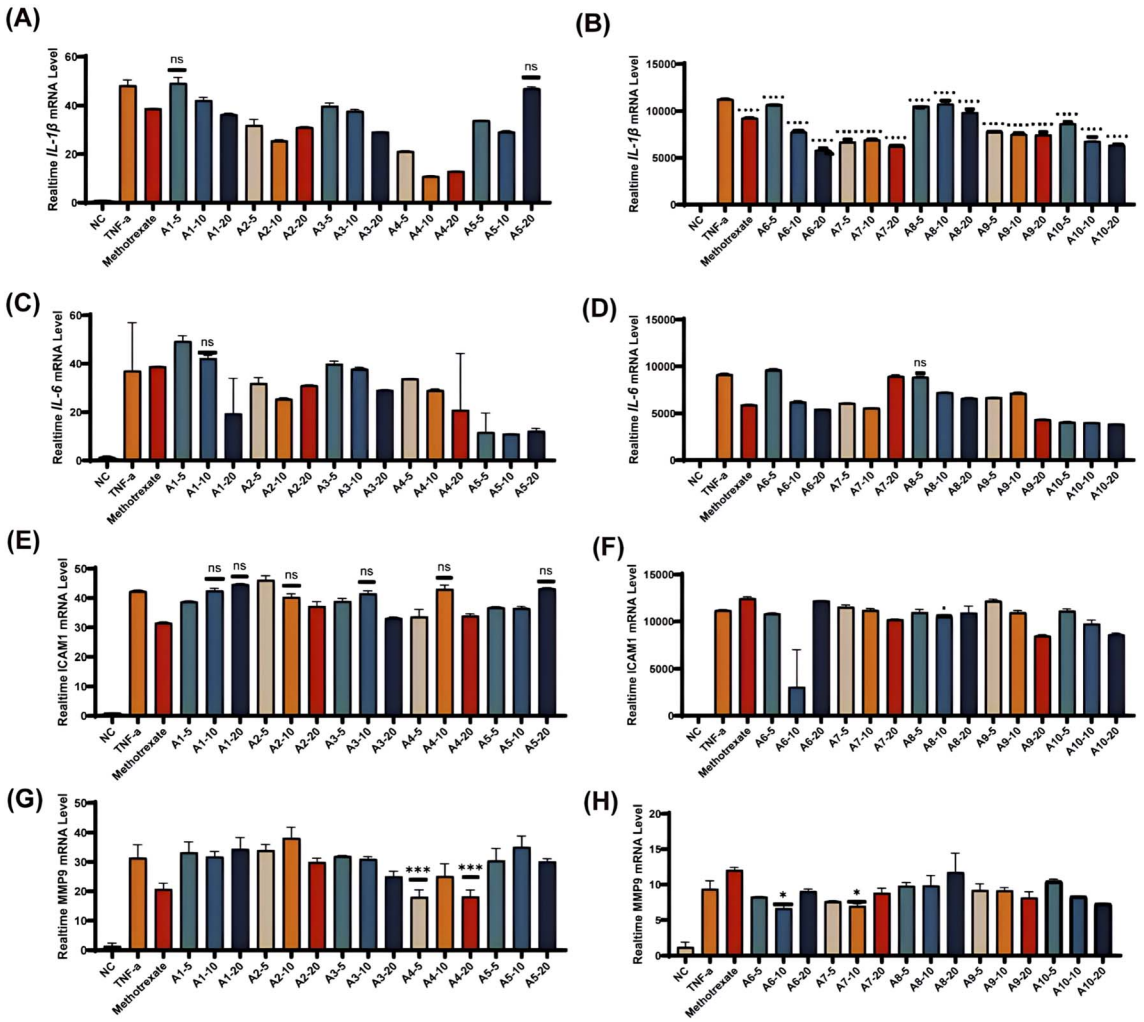

Fig. 1 Screening of indobufen-modified derivatives. (A) IL-1β mRNA levels in cells treated with test compounds (**A1–A5** series) relative to NC (normal control) and TNF-α (positive control) groups. (B) IL-1β mRNA levels in cells treated with test compounds (**A6–A10** series) relative to NC and TNF-α control groups. (C) IL-6 mRNA levels in cells treated with test compounds (**A1–A5** series) relative to NC and TNF-α control groups. (D) IL-6 mRNA levels in cells treated with test compounds (**A6–A10** series) relative to NC and TNF-α control groups. (E) ICAM1 mRNA levels in cells treated with test compounds (**A1–A5** series) relative to NC and TNF-α control groups. (F) ICAM1 mRNA levels in cells treated with test compounds (**A6–A10** series) relative to NC and TNF-α control groups. (G) MMP9 mRNA levels in cells treated with test compounds (**A1–A5** series) relative to NC and TNF-α control groups. (H) MMP9 mRNA levels in cells treated with test compounds (**A6–A10** series) relative to NC and TNF-α control groups. Data are presented as mean ± SD; ns = not significant, *$p < 0.05$, **$p < 0.01$, ***$p < 0.001$ *vs.* TNF-α group.

potential in inflammation-associated osteoclastogenesis and bone resorption.

2.3 Extended inflammatory profiling

To further prioritize lead candidates after the initial screen (Fig. 1), we expanded transcriptional profiling to three representative derivatives (**A1–A3**) and a broader panel of cytokine and chemokine genes. FLS cells were exposed to **A1–A3** at 10 and 20 μM, and gene expression changes were benchmarked against a negative control (NC) and an LPS-treated positive control processed in parallel. This design allowed us to distinguish compounds that are intrinsically pro-inflammatory from those with a comparatively low inflammatory liability. As shown in Fig. 2A–C, LPS markedly increased the transcription of IL-6, IL-1α, and IL-1β relative to NC, confirming robust inflammatory activation. At both concentrations tested, **A1** resulted in minimal induction of the measured cytokines. In contrast, **A3** triggered a strong inflammatory response, particularly at 20 μM, at which IL-6 and IL-1α transcript levels reached or surpassed those observed in LPS-treated cells. The effects of A2 were moderate relative to **A1** and **A3**. This pattern suggests that cytokine responses differ in a structure-dependent manner among the three compounds.A similar pattern was observed for chemokine-related genes (CCL5, CCL7, CXCL9, and CXCL10; Fig. 2D–G). LPS significantly elevated CCL5, CCL7, and CXCL10 compared with NC. Among the derivatives, **A3** again produced the strongest and most dose-dependent induction of CCL5 and CCL7, whereas **A2** and **A3** more prominently increased CXCL10. In contrast, **A1** triggered comparatively modest chemokine responses. CXCL9 showed only limited variation across

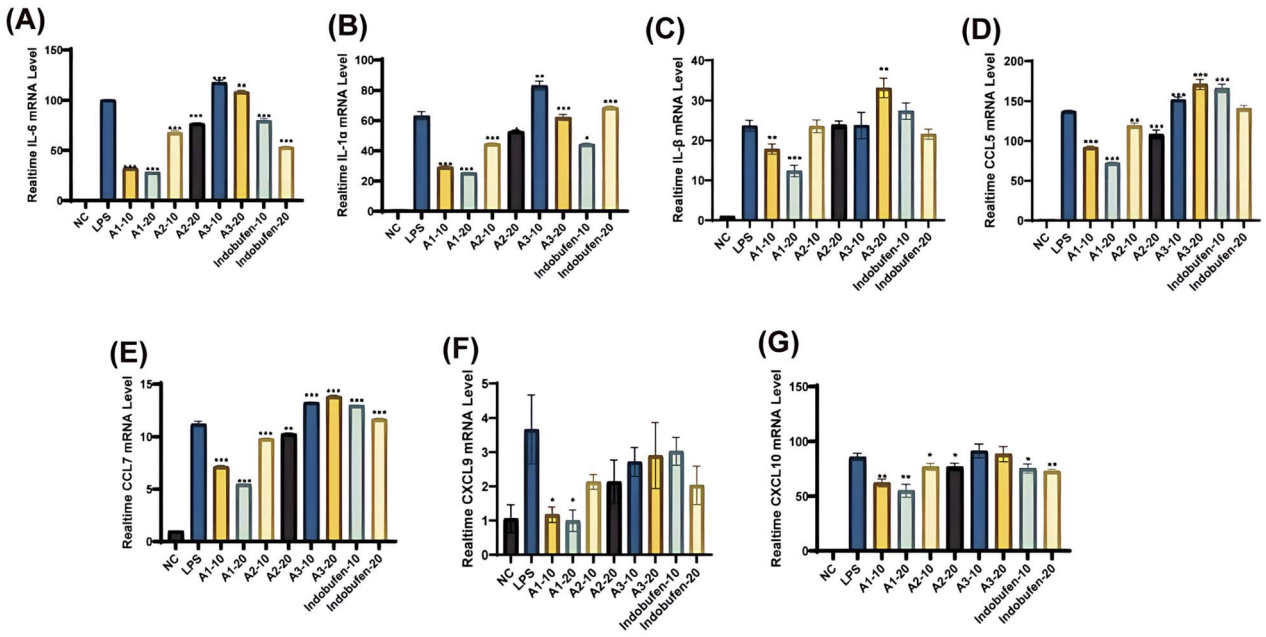

Fig. 2 **A1–A3** differentially regulate inflammatory cytokine and chemokine gene expression in LPS-stimulated FLS cells. (A) IL-6 mRNA expression levels in NC, LPS, test compound (**A1–A3** series), and indobufen treatment groups. (B) IL-1α mRNA expression levels in NC, LPS, test compound (**A1–A3** series), and indobufen treatment groups. (C) IL-1β mRNA expression levels in NC, LPS, test compound (**A1–A3** series), and indobufen treatment groups. (D) CCL5 mRNA expression levels in NC, LPS, test compound (**A1–A3** series), and indobufen treatment groups. (E) CCL7 mRNA expression levels in NC, LPS, test compound (**A1–A3** series), and indobufen treatment groups. (F) CXCL9 mRNA expression levels in NC, LPS, test compound (**A1–A3** series), and indobufen treatment groups. (G) CXCL10 mRNA expression levels in NC, LPS, test compound (**A1–A3** series), and indobufen treatment groups. Data are presented as mean ± SD; $*p < 0.05$, $**p < 0.01$, $***p < 0.001$ *vs.* LPS group.

treatments, suggesting selective regulation of chemokine subtypes rather than a uniform amplification of all chemotactic signals. Indobufen (10 and 20 μM) was included as a reference compound and induced only moderate transcriptional changes across the cytokine and chemokine panel, remaining consistently below the responses observed with **A3** at equivalent

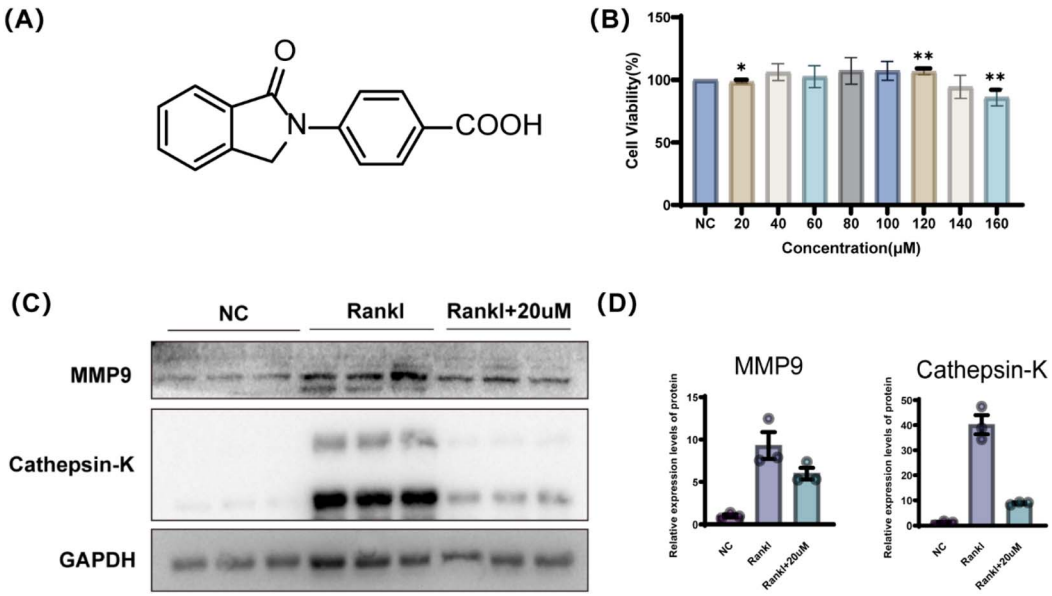

Fig. 3 Chemical structure, cytotoxicity evaluation, and inhibitory effects of **A1** on osteoclast functional protein expression. (A) The chemical structure of **A1**. (B) Cytotoxicity of **A1** at concentrations from 20 to 160 μM in RAW264.7 cell. (C) Representative western blot images showing the expression of MMP9 and cathepsin-K in RAW264.7 cells treated with RANKL in the presence or absence of **A1** (20 μM). GAPDH was used as a loading control. (D) Quantitative densitometric analysis of MMP9 and cathepsin-K protein levels normalized to GAPDH. Data are presented as mean ± SD ($n = 3$). $*P < 0.05$, $**P < 0.01$.

concentrations. Collectively, this extended profiling indicates that **A1** has the lowest inflammatory liability among **A1–A3** in FLS cells, supporting its selection for subsequent osteoclast-focused assays, therefore we focused on **A1** to avoid confounding pro-inflammatory activation in downstream osteoclastogenesis assays.

2.4 A1 exhibits favorable cellular safety and suppresses osteoclast functional protein expression

To investigate the biological activity of the indobufen-modified compound **A1**, its chemical structure is shown in Fig. 3A. The cytotoxicity of **A1** was first evaluated using a CCK-8 assay to determine an appropriate concentration range for subsequent experiments. As shown in Fig. 3B, treatment with **A1** at concentrations ranging from 20 to 120 μM did not result in significant cytotoxic effects, with cell viability remaining above 90% compared with the NC group. **A1** did not compromise RAW264.7 cell viability at concentrations up to 120 μM, whereas exposure to 140 or 160 μM resulted in a pronounced viability loss, consistent with dose-dependent cytotoxicity. Non-cytotoxic concentrations of compound **A1** were therefore selected for mechanistic analysis, given that osteoclast-mediated bone resorption is closely linked to functional protease expression. We employed western blotting to determine how **A1** modulates the expression levels of RANKL-induced matrix metalloproteinase 9 (MMP9) and cathepsin K. As shown in Fig. 3C, RANKL stimulation markedly increased the levels of both proteins relative to the negative control (NC) group, whereas treatment with 20 μmol L^{-1} **A1** substantially attenuated this induction. Densitometric analysis further confirmed reduced MMP9 and cathepsin K expression in **A1**-treated cells compared with RANKL-only controls (Fig. 3D). These findings indicate that **A1** suppresses osteoclast functional protein expression under non-cytotoxic conditions, supporting a mechanism independent of non-specific cytotoxic effects.

2.5 A1 disrupts F-actin ring formation during RANKL-induced osteoclast differentiation

To further investigate the effects of **A1** on osteoclast maturation, F-actin organization was examined by immunofluorescence staining in RAW264.7 cells subjected to RANKL-induced osteoclastogenesis. As shown in Fig. 4A, cells in the NC group exhibited a relatively uniform cortical distribution of F-actin without the formation of distinct actin ring structures. In contrast, RANKL stimulation (RANKL group) induced the formation of large, well-defined F-actin rings accompanied by multinucleated cells, which are characteristic features of mature osteoclasts. Treatment with **A1** resulted in a marked disruption of RANKL-induced F-actin ring formation in a concentration-dependent manner. At 10 μM, **A1** partially impaired the integrity of F-actin rings, with fewer and less continuous ring structures observed compared with the RANKL group. Increasing the concentration of **A1** to 20 μM further attenuated F-actin ring formation, accompanied by markedly reduced cell fusion and disorganized cytoskeletal structures.

3 Materials and methods

3.1 Chemical synthesis of indobufen derivatives

3.1.1 General procedure for synthesis of A1 to A4. To a solution of *o*-carboxybenzaldehyde (3.33 mmol, 1.0 equiv., 0.50 g) in 5 mLof dichloromethane at 25 °C were added

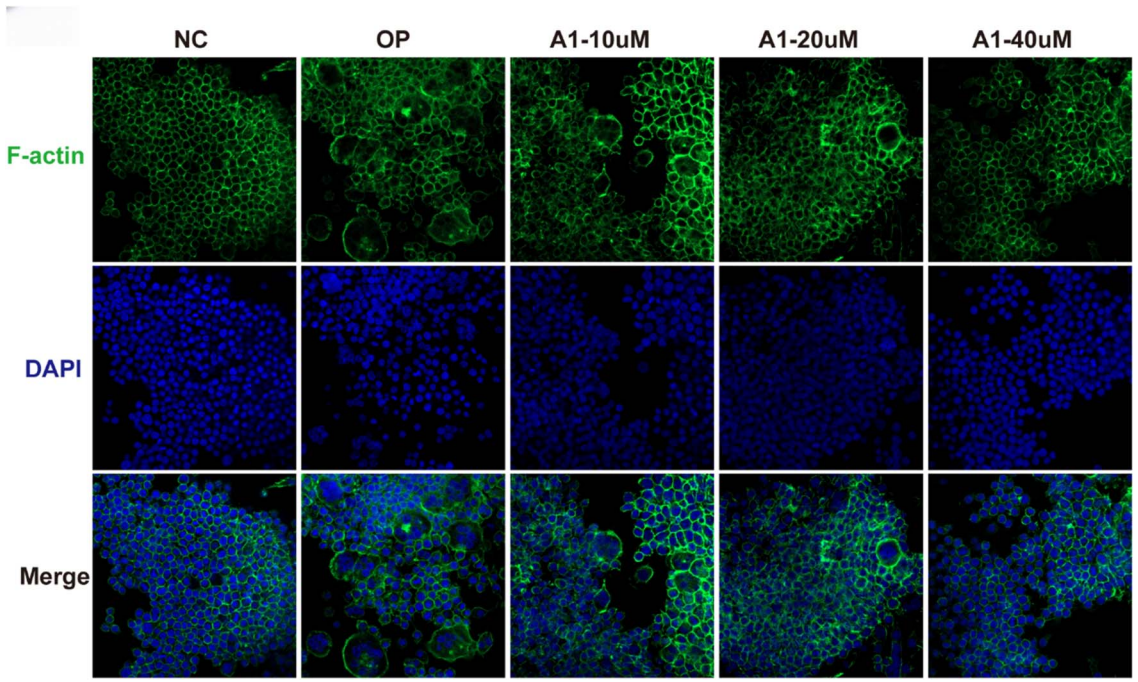

Fig. 4 Inhibition of F-Actin Ring Assembly by Indobufen Derivative **A1** During RANKL-Mediated Osteoclast Differentiation.

substituted anilines (1.1 equiv.) and diethyl 2,6-dimethyl-1,4-dihydro-3,5- pyridinedicarboxylate (3.99 mmol, 1.2 equiv., 1.0 g). The resulting suspension was stirred for 2 hours. Upon completion, the solvent was removed under reduced pressure, and the residue was dried under high vacuum and used directly in the next step. To a solution of **3a** to **3d** (1.0 equiv.) in 4 mL of anhydrous methanol at 25 °C was slowly added 2 mL of 2 M aqueous sodium hydroxide solution. The resulting suspension was stirred for 2 hours, and the reaction progress was monitored by thin-layer chromatography (TLC) until completion. Subsequently, 6 mL of ethanol was added to the reaction mixture, followed by adjusting the pH of the system to acidic (pH = 3) with dilute hydrochloric acid, and solid precipitation was observed. After stirring continuously for 10 minutes, the solid was collected by filtration, washed with a small amount of cold ethanol, and dried to afford product **A1** to **A4** as a solid.

3.1.2 General procedure for synthesis of A5 to A10. To a solution of Indobufen (1.69 mmol, 1.0 equiv., 0.50 g) in 5 mL of anhydrous DMF at 25 °C were sequentially added DIPEA (5.07 mmol, 3.0 equiv., 0.65 g) and HATU (1.85 mmol, 1.1 equiv., 0.70 g). The mixture was stirred for 10–15 min for activation. Then, amine derivatives (3.0 equiv.) was added dropwise over 15–20 min. After the addition was complete, the reaction mixture was stirred at 25 °C for 12–16 h, and monitored by thin-layer chromatography (TLC) until indobufen was completely consumed. The reaction solution was poured into saturated aqueous sodium chloride, and extracted with ethyl acetate (3 × 15 mL). The combined organic phases were dried over anhydrous sodium sulfate and concentrated under reduced pressure to afford compound **A5** to **A10** as a solid. Detailed experimental procedures, characterization data, and NMR spectra for all compounds are provided in the SI.

3.2 Cell culture

Fibroblast-like synoviocytes (FLS) cells were cultured in Dulbecco's Modified Eagle Medium (DMEM, high glucose) supplemented with 10% fetal bovine serum (FBS), 100 U mL^{-1} penicillin, and 100 μg mL^{-1} streptomycin. RAW264.7 cells were maintained in DMEM containing 10% FBS and antibiotics under the same conditions. All cells were incubated at 37°Cin a humidified atmosphere with 5% CO_2. Culture media were refreshed every 2–3 days, and cells were passaged upon reaching approximately 80% confluence. RAW264.7 cells were selected due to their well-established capacity to differentiate into osteoclast-like cells upon receptor activator of nuclear factor-κB ligand (RANKL) stimulation,[24] making them a widely accepted *in vitro* model for osteoclastogenesis studies.[25] RAW264.7 mouse monocyte/macrophage cell (PubMed ID: 23430347) and Human primary spondylitis hip joint synovial fibroblasts (Cat No. HUM-iCell-s010RA-1) were purchased from iCell Bioscience Inc. (Shanghai, China). Recombinant mouse RANKL (Cat No. PRP1114) was purchased from Proteintech Group, Inc. (Wuhan, China). The following primary antibodies were used in this study: anti-cathepsin K (Cat No. 11239-1-AP, Proteintech), anti-MMP-9 (Cat No. 10375-2-AP, Proteintech), and anti-GAPDH (Cat No. 60004-1-Ig, Proteintech).

3.3 Inflammatory stimulation and compound screening in FLS cells

FLS were seeded in plates and allowed to adhere overnight. Cells were pretreated with each indobufen-derived compound (**A1–A10**, 20 μM; final DMSO ≤ 0.1%) for 1 h and then exposed to lipopolysaccharide (LPS) to induce an inflammatory response. After 6 h stimulation, total RNA was harvested for RT-qPCR analysis of Il1b, Il6, Mmp9 and Icam1. For the extended cytokine/chemokine panel, FLS were treated with **A1–A3** or indobufen at 10 and 20 μM, and LPS-stimulated in parallel. LPS alone served as the positive control and vehicle-treated cells served as the negative control.

3.4 Quantitative PCR analysis

Total RNA was extracted from FLS or RAW264.7 cells using TRIzol (or an equivalent commercial reagent) according to the manufacturer's instructions. RNA concentration and purity were assessed by spectrophotometry, and equal amounts of RNA were reverse-transcribed to cDNA using a commercial reverse transcription kit. RT-qPCR was performed using SYBR Green chemistry on a real-time PCR system. For FLS, inflammatory and matrix-related genes (Il1b, Il6, Il1a, Mmp9, Icam1, Ccl5, Ccl7, Cxcl9 and Cxcl10) were quantified. For RAW264.7 cells, osteoclast-related genes (Acp5/TRAP, Nfatc1 and Ctsk) were quantified when indicated. GAPDH was used as the internal reference gene. Relative expression was calculated using the 2-ΔΔCt method, normalized to the vehicle control group. Each sample was run in technical triplicate, and all experiments were repeated in at least three independent biological replicates.

3.5 Cell viability assay (CCK-8)

Cell viability was evaluated using the Cell Counting Kit-8 (CCK-8) assay. FLS or RAW264.7 cells were seeded in 96-well plates and allowed to adhere overnight, then treated with test compounds (vehicle control: DMSO ≤ 0.1%). For the **A1** dose-range assessment, RAW264.7 cells were exposed to **A1** (20–160 μM) for 24 h before CCK-8 measurement. Following treatment, 10 μL of CCK-8 reagent was added to each well and incubated at 37 °C for 1–2 h. Absorbance was measured at 450 nm using a microplate reader. Cell viability was calculated as a percentage relative to the untreated control group. Experiments were performed in triplicate and repeated independently at least three times. The CCK-8 assay was chosen due to its high sensitivity and reproducibility in assessing cellular metabolic activity.[26]

3.6 RANKL-induced osteoclastogenesis in RAW264.7 cells

RAW264.7 cells were used to establish an *in vitro* osteoclastogenesis model. Cells were seeded in culture plates (*e.g.*, 6-well plates for protein analysis and coverslips in 24-well plates for imaging) and stimulated with recombinant mouse RANKL (typically 50 ng mL^{-1}) to induce osteoclast differentiation. Test compounds were added at the start of induction and maintained throughout differentiation with medium changes every 48 h. For the mechanistic evaluation of **A1**, cells were treated

with **A1** at the indicated concentrations (10, 20 or 40 μM for F-actin ring analysis; 20 μM for western blotting unless otherwise stated). Differentiation was monitored by the appearance of multinucleated osteoclast-like cells and by the induction of osteoclast markers at the mRNA and/or protein level.

3.7 Western blot analysis

Western blotting was performed to analyze osteoclast functional proteins and signaling molecules. Following treatment, RAW264.7 cells were lysed in RIPA buffer supplemented with protease and phosphatase inhibitors. Protein concentrations were determined using a BCA assay. Membranes were probed with primary antibodies against MMP9, cathepsin-K (CTSK) and GAPDH (loading control). When indicated, antibodies against NF-κB/MAPK pathway components and NFATc1 were also used. Equal amounts of protein were separated by SDS–PAGE and transferred onto polyvinylidene fluoride (PVDF) membranes. After blocking with 5% non-fat milk, membranes were incubated overnight at 4 °Cwith primary antibodies targeting osteoclast-related signaling proteins, including components of the NF-κB pathway, MAPK pathway, and NFATc1. Membranes were then incubated with appropriate horseradish peroxidase–conjugated secondary antibodies and visualized using an enhanced chemiluminescence detection system. Protein band intensities were quantified using ImageJ software and normalized to the corresponding loading control. Western blot analysis was conducted following established protocols for investigating osteoclast-related signaling mechanisms.[27]

3.8 Immunofluorescence and confocal microscopy

For cytoskeletal visualization, F-actin ring formation was assessed by phalloidin staining. RAW264.7 cells cultured on glass coverslips were induced with RANKL in the presence or absence of **A1**, fixed with 4% paraformaldehyde, permeabilized with 0.1% Triton X-100, and blocked with bovine serum albumin. Cells were stained with fluorescent phalloidin to label F-actin and counterstained with DAPI to visualize nuclei. Images were acquired using a confocal laser scanning microscope under identical settings for all groups. F-actin ring integrity and the number of multinucleated cells were quantified using ImageJ in a blinded manner from multiple random fields per condition. Where indicated, immunofluorescence staining for protein targets was performed using primary antibodies followed by fluorophore-conjugated secondary antibodies. Immunofluorescence provides spatial confirmation of molecular and morphological changes during osteoclast differentiation and drug intervention.[28]

3.9 Statistical analysis

All experimental assays were conducted with a minimum of three independent repetitions. Results are presented as the arithmetic mean the standard deviation. Statistical evaluations were carried out employing appropriate software packages. For comparisons involving multiple experimental groups, a one-way analysis of variance was performed, followed by suitable *post hoc* tests as indicated. A probability value of was considered to denote a statistically significant difference.

4 Conclusions

In conclusion, this study designed and synthesized a series of novel indobufen derivatives based on drug repurposing and scaffold hopping medicinal chemistry strategies. Through the establishment of a hierarchical phenotypic screening model encompassing inflammatory microenvironment regulation and bone resorption endpoint blockade, we successfully identified the lead compound **A1**. Experimental data demonstrate that **A1** exhibits unique dual pharmacological activities in *in vitro* models. On one hand, **A1** significantly inhibited the secretion of pro-inflammatory factors, including IL-1 and IL-6, from fibroblast-like synoviocytes, thereby interrupting the pathological drive of inflammation on bone remodeling. On the other hand, **A1** directly targeted the RANKL-induced osteoclast differentiation program. Within a clear therapeutic window, **A1** not only downregulated the expression of NFATc1 and its downstream effector proteins but also markedly disrupted cytoskeletal F-actin ring assembly, thereby blocking bone resorption from both transcriptional and structural dimensions. These findings confirm the potential of the indobufen scaffold, following rational chemical modification, to effectively target the immuno–skeletal interface. As a small-molecule inhibitor with a novel dual-target mechanism, **A1** extends beyond the simple cyclooxygenase–inhibitory activity of its parent compound and provides a valuable candidate and experimental foundation for clinical intervention in secondary osteoporosis associated with rheumatoid arthritis or postmenopausal inflammatory bone loss.

Author contributions

D. Yuan, L. Chen and X. Huang performed experiments and synthesis of indobufen derivatives. Z. Meng and J. Zhang supervised the project and prepared the manuscript. All authors discussed the results and commented on the manuscript.

Conflicts of interest

The authors declare no competing financial interest.

Data availability

The data underlying this study are available in the published article and supporting information (SI). Supplementary information: materials, experimental details and NMR spectra for the synthesis of indobufen derivatives. See DOI: https://doi.org/10.1039/d6ra01985d.

Acknowledgements

This work was supported by the Project of Natural Science Foundation of Jiangxi Province (20252BAC200103), (20242BAB21036) and (20232BAB216135).

Notes and references

1 S. Khosla and L. C. Hofbauer, Osteoporosis treatment: recent developments and ongoing challenges, *Lancet Diabetes Endocrinol.*, 2017, **5**, 898–907.
2 B. Liang, G. Burley, S. Lin and Y. C. Shi, Osteoporosis pathogenesis and treatment: existing and emerging avenues, *Cell. Mol. Biol. Lett.*, 2022, **27**, 72.
3 N. Salari, H. Ghasemi, L. Mohammadi, *et al.*, The global prevalence of osteoporosis in the world: a comprehensive systematic review and meta-analysis, *J. Orthop. Surg. Res.*, 2021, **16**, 609.
4 J. Wang, B. Shu, D. Z. Tang, C. G. Li, X. W. Xie, L. J. Jiang, X. B. Jiang, B. L. Chen, X. C. Lin, X. Wei, X. Y. Leng, Z. Y. Liao, B. L. Li, Y. Zhang, X. J. Cui, Q. Zhang, S. Lu, Q. Shi and Y. J. Wang, The prevalence of osteoporosis in China, a community based cohort study of osteoporosis, *Front. Public Health*, 2023, **11**, 1084005.
5 Y. Wang, Y. Tao, M. E. Hyman, J. Li and Y. Chen, Osteoporosis in china, *Osteoporosis Int.*, 2009, **20**, 1651–1662.
6 S. Meng, M. Tong, Y. Yu, Y. Cao, B. Tang, X. Shi and K. Liu, The prevalence of osteoporotic fractures in the elderly in China: a systematic review and meta-analysis, *J. Orthop. Surg. Res.*, 2023, **18**, 536.
7 Y. Wu, H. Ai, Y. Xi, P. Yin, Y. Qu, J. Xu, C. Dou and F. Luo, Reduced osteoclast-derived apoptotic bodies in bone marrow characterizes the pathological progression of osteoporosis, *Cell Death Discovery*, 2023, **9**, 135.
8 D. S. Amarasekara, H. Yun, S. Kim, N. Lee, H. Kim and J. Rho, Regulation of Osteoclast Differentiation by Cytokine Networks, *Immune Netw*, 2018, **18**, e8.
9 J. H. Park, N. K. Lee and S. Y. Lee, Current Understanding of RANK Signaling in Osteoclast Differentiation and Maturation, *Mol. Cells*, 2017, **40**, 706–713.
10 T. Matsumoto and I. Endo, RANKL as a target for the treatment of osteoporosis, *J. Bone Miner. Metab.*, 2021, **39**, 91–105.
11 S. Khosla and D. G. Monroe, Regulation of Bone Metabolism by Sex Steroids, *Cold Spring Harb. Perspect. Med.*, 2018, **8**, a031211.
12 W. J. Boyle, W. S. Simonet and D. L. Lacey, Osteoclast differentiation and activation, *Nature*, 2003, **423**, 337–342.
13 H. Takayanagi, Osteoimmunology and the effects of the immune system on bone, *Nat. Rev. Rheumatol.*, 2009, **5**, 667–676.
14 E. Shane, D. Burr, P. R. Ebeling, B. Abrahamsen, R. A. Adler, T. D. Brown, A. M. Cheung, F. Cosman, J. R. Curtis, R. Dell, D. Dempster, T. A. Einhorn, H. K. Genant, P. Geusens, K. Klaushofer, K. Koval, J. M. Lane, F. McKiernan, R. McKinney, A. Ng, J. Nieves, R. O'Keefe, S. Papapoulos, H. T. Sen, M. C. H. van der Meulen, R. S. Weinstein and M. Whyte, American Society for Bone and Mineral Research. Atypical subtrochanteric and diaphyseal femoral fractures: report of a task force of the American Society for Bone and Mineral Research, *J. Bone Miner. Res.*, 2010, **25**, 2267–2294.
15 I. R. Reid, Short-term and long-term effects of osteoporosis therapies, *Nat. Rev. Endocrinol.*, 2015, **11**, 418–428.
16 R. M. Neer, C. D. Arnaud, J. R. Zanchetta, R. Prince, G. A. Gaich, J. Y. Reginster, A. B. Hodsman, E. F. Eriksen, S. Ish-Shalom, H. K. Genant, O. Wang and B. H. Mitlak, Effect of parathyroid hormone (1-34) on fractures and bone mineral density in postmenopausal women with osteoporosis, *N. Engl. J. Med.*, 2001, **344**, 1434–1441.
17 S. Pushpakom, F. Iorio, P. A. Eyers, K. J. Escott, S. Hopper, A. Wells, A. Doig, T. Guilliams, J. Latimer, C. McNamee, A. Norris, P. Sanseau, D. Cavalla and M. Pirmohamed, Drug repurposing: progress, challenges and recommendations, *Nat. Rev. Drug Discovery*, 2019, **18**, 41–58.
18 N. Bhana and K. J. McClellan, Indobufen: an updated review of its use in the management of atherothrombosis, *Drugs Aging*, 2001, **18**, 369–388.
19 A. R. Brash, Arachidonic acid as a bioactive molecule, *J. Clin. Invest.*, 2001, **107**, 1339–1345.
20 Q. Lu, J. Xu, H. Jiang, Q. Wei, R. Huang and G. Huang, The bone-protective mechanisms of active components from TCM drugs in rheumatoid arthritis treatment, *Front. Pharmacol*, 2022, **13**, 1000865.
21 T. Yang, W. W. Chen, K. Gan, C. F. Wang, X. X. Xie, Y. G. Su, H. Y. Lian, J. Xu, J. M. Zhao and Q. Liu, Myrislignan targets extracellular signal-regulated kinase (ERK) and modulates mitochondrial function to dampen osteoclastogenesis and ovariectomy-induced osteoporosis, *J. Transl. Med.*, 2023, **21**, 839.
22 H. Huynh and Y. Wan, mTORC1 impedes osteoclast differentiation *via* calcineurin and NFATc1, *Commun. Biol.*, 2018, **1**, 29.
23 T. S. Suda, K. Kobayashi, E. Jimi, N. Udagawa and N. Takahashi, The molecular basis of osteoclast differentiation and activation, *Novartis Found. Symp.*, 2001, **232**, 235–247.
24 P. Collin-Osdoby and P. Osdoby, RANKL-mediated osteoclast formation from murine RAW 264.7 cells, *Methods Mol. Biol.*, 2012, **816**, 187–202.
25 W. J. Boyle, W. S. Simonet and D. L. Lacey, Osteoclast differentiation and activation, *Nature*, 2003, **423**, 337–342.
26 M. Ishiyama, Y. Miyazono, K. Sasamoto, Y. Ohkura and K. Ueno, A highly water-soluble disulfonated tetrazolium salt as a chromogenic indicator for NADH as well as cell viability, *Talanta*, 1997, **44**, 1299–1305.
27 Z. H. Lee and H. H. Kim, Signal transduction by receptor activator of nuclear factor kappa B in osteoclasts, *Biochem. Biophys. Res. Commun.*, 2003, **305**, 211–214.
28 S. Epsley, S. Tadros, A. Farid, D. Kargilis, S. Mehta and C. S. Rajapakse, The Effect of Inflammation on Bone, *Front. Physiol.*, 2021, **11**, 511799.